Supporting information

Facile encapsulation strategy for uniformly-dispersed catalytic nanoparticle/carbon nanofiber toward advanced Zn-air battery

Seong Woon Yoon[†,a,b], *Dae-Kwon Boo*[†,c,d], *Hyunmin Na*[c,d], *Tae Yoen Kim*[a,b], *Hyunsoo Chang*[a,b], *Ji Sung Park*[a,b], *Su-Ho Cho*[e], *Ji-Won Jung*[d,*], *Hyeong Min Jin*[a,b,*]

[a]Department of Organic Materials Engineering, Chungnam National University, Daejeon 34134, Republic of Korea

[b]Department of Materials Science and Engineering, Chungnam National University, Daejeon 34134, Republic of Korea

[c]School of Materials Science and Engineering, University of Ulsan, Techno Saneop-ro 55 Beon-gil, Nam-gu, Ulsan 44776, Republic of Korea

[d]Department of Materials Science and Engineering, Konkuk University, 120, Neungdong-ro, Gwangjin-gu, Seoul 05029, Republic of Korea

[e]National Nano Fab Center (NNFC), 291 Daehak-ro, Yuseong-gu, Daejeon 34141, Republic of Korea

†Contributed equally to this work.
*Correspondence to: jwjung4@konkuk.ac.kr; hyeongmin@cnu.ac.kr

This file includes:
Figs. S1 to S18
Table S1 to S3

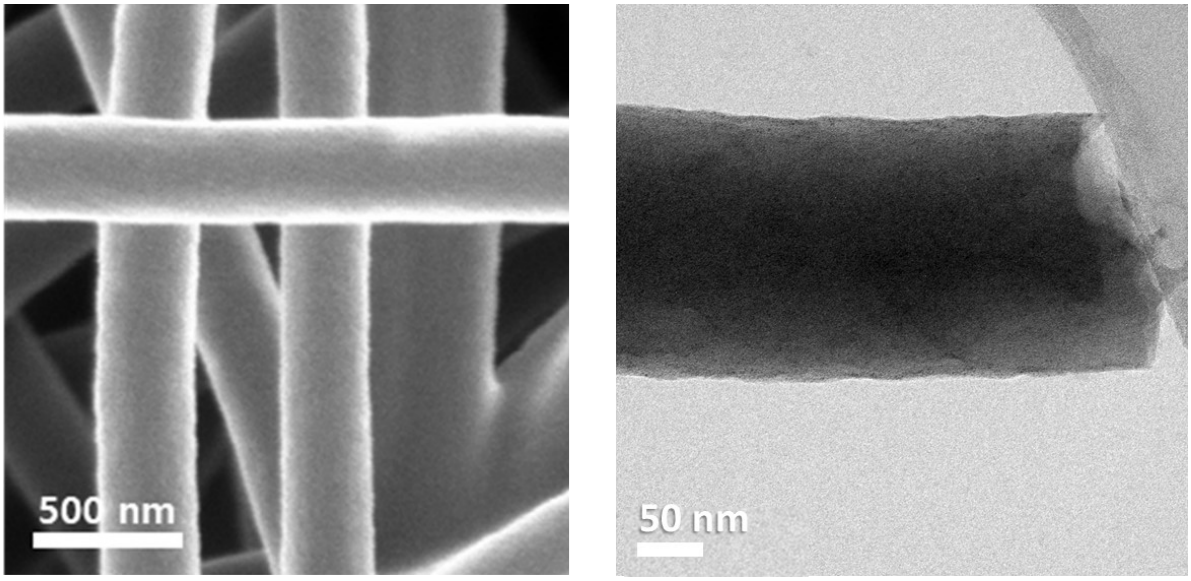

Fig. S1. (a) SEM image and (b) TEM image of neat CNF (without P4VP blending) after Ir loading and carbonization.

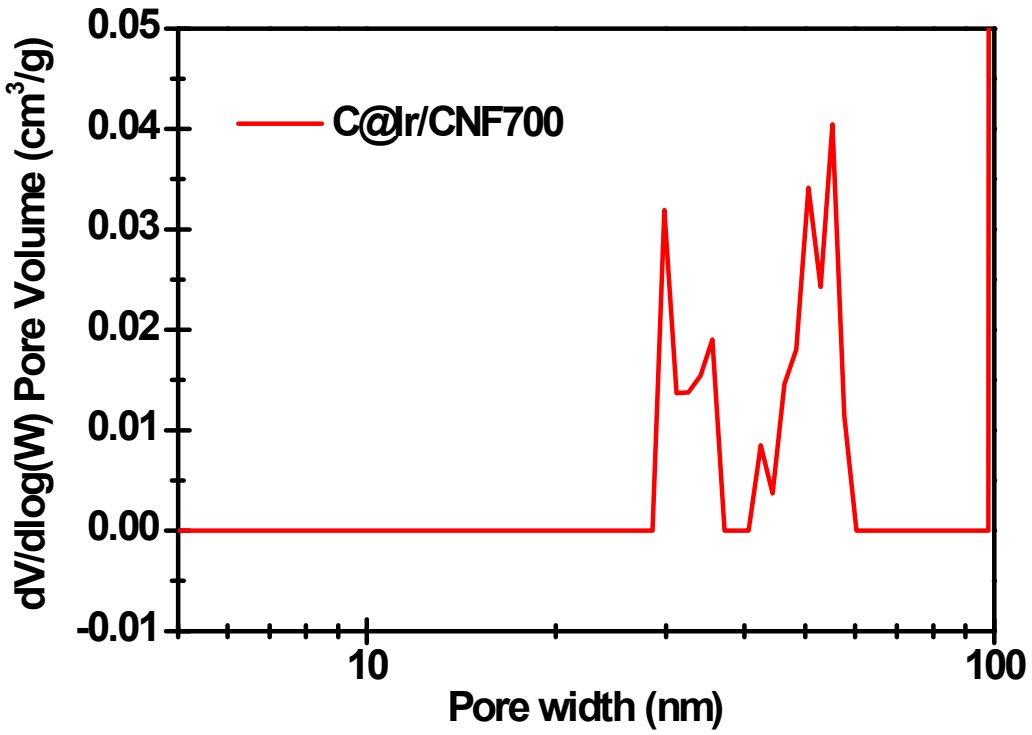

Fig. S2. BJH analysis to evaluate the pore size and volume of C@Ir/CNF700.

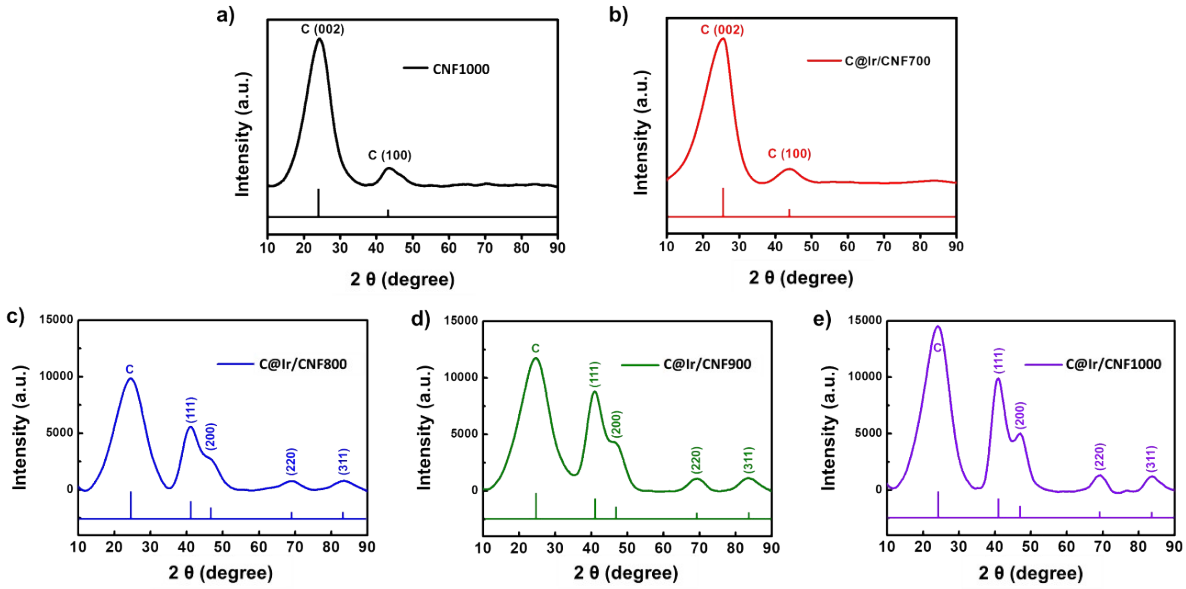

Fig. S3. XRD crystal peaks as a function of carbonization temperature for (a) CNF1000 (non-loading CNF sample), (b) C@Ir/CNF700, (c) C@Ir/CNF800, (d) C@Ir/CNF900, and (e) C@Ir/CNF1000.

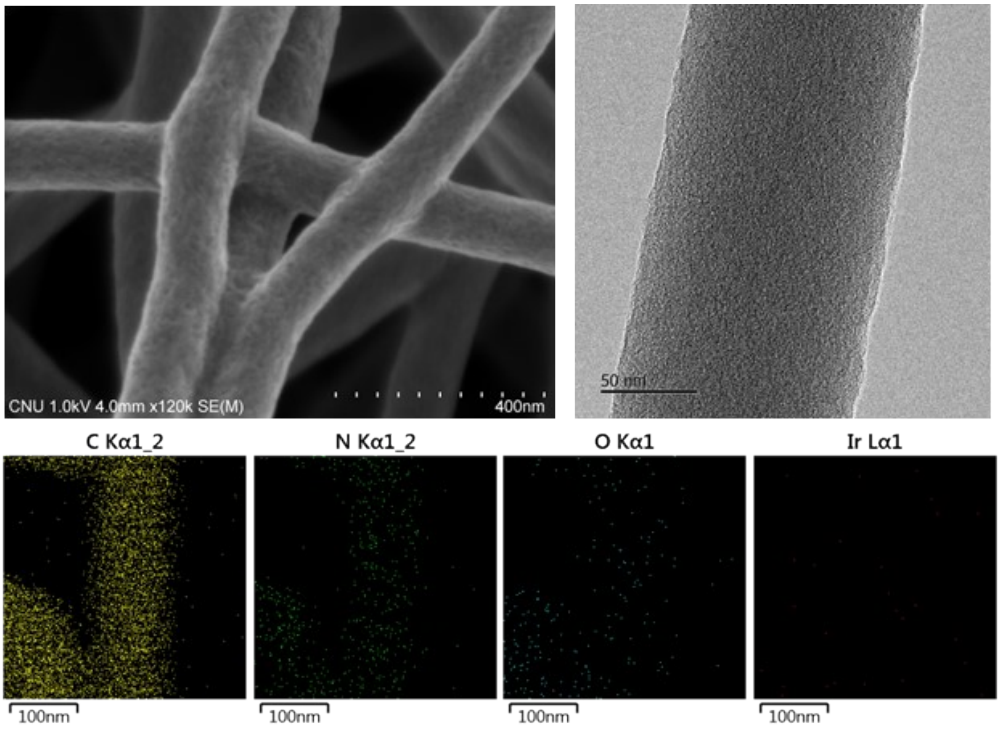

	C1s	Ir4f	N1s	O1s
At. %	93.8	0	3.33	2.87
Wt. %	92.41	0	3.83	3.77

Fig. S4. SEM, TEM, EDS, and XPS data of C/CNF1000.

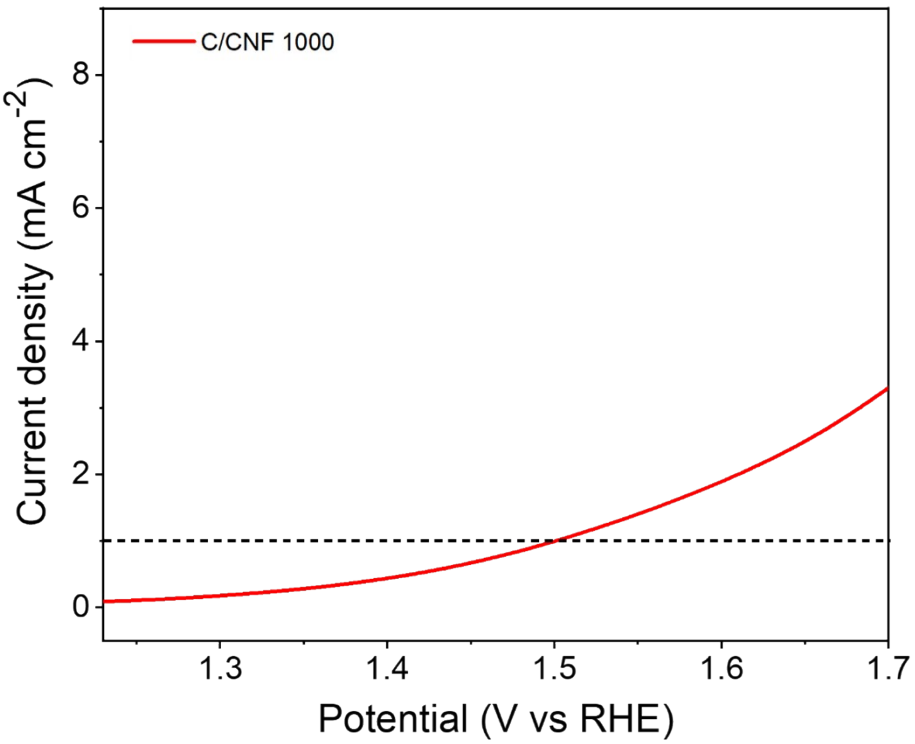

Fig. S5. OER-LSV curves of C/CNF1000 in 1 M KOH at a scan rate of 5 mV s^{-1} from 1.2 to 1.7 V vs. RHE.

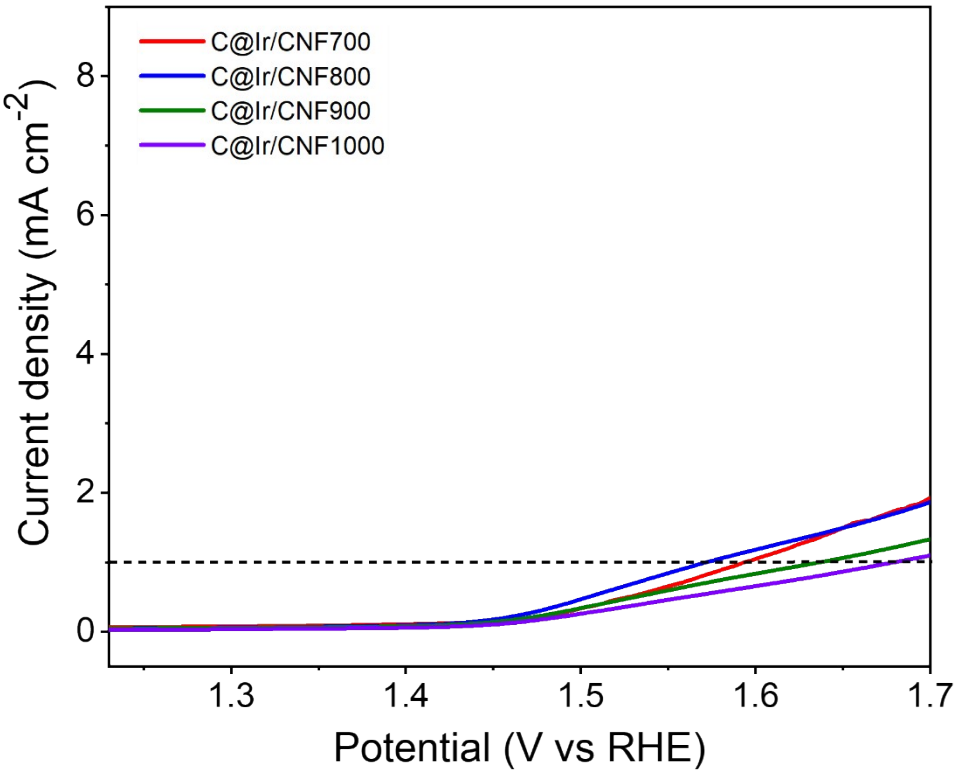

Fig. S6. OER-LSV curves of C@Ir/CNF700, C@Ir/CNF800, C@Ir/CNF900, and C@Ir/CNF1000 without CM (Ketjen Black) in 1 M KOH at a scan rate of 5 mV s^{-1} from 1.2 to 1.7 V vs. RHE.

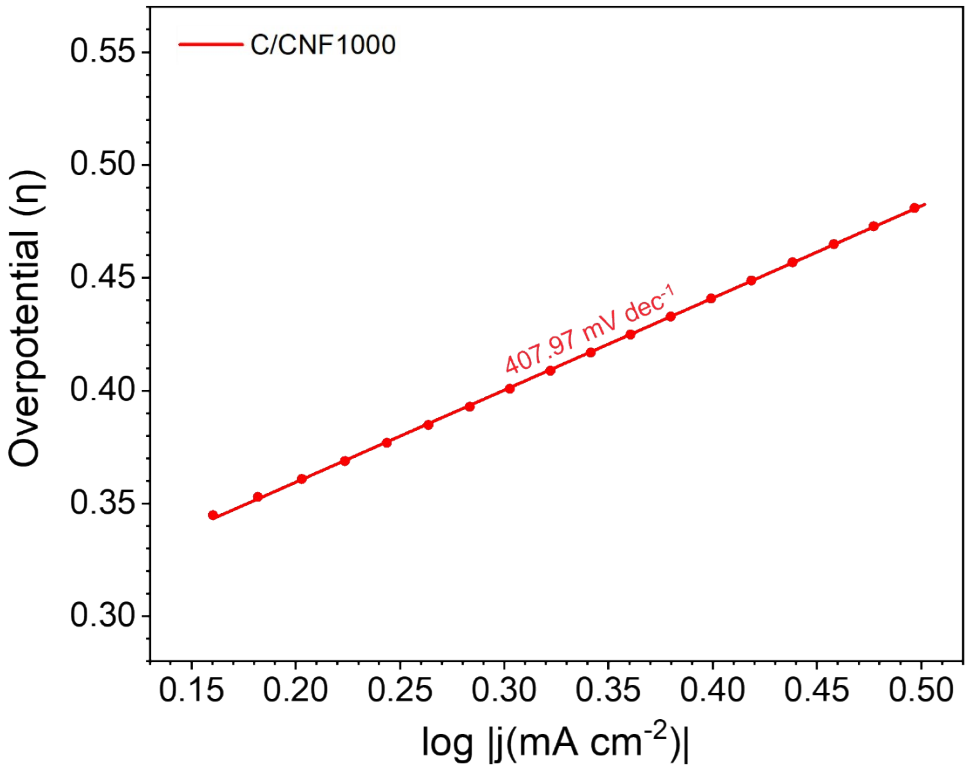

Fig. S7. Tafel plots of C/CNF1000 derived from the OER-LSV curves in Fig. S5.

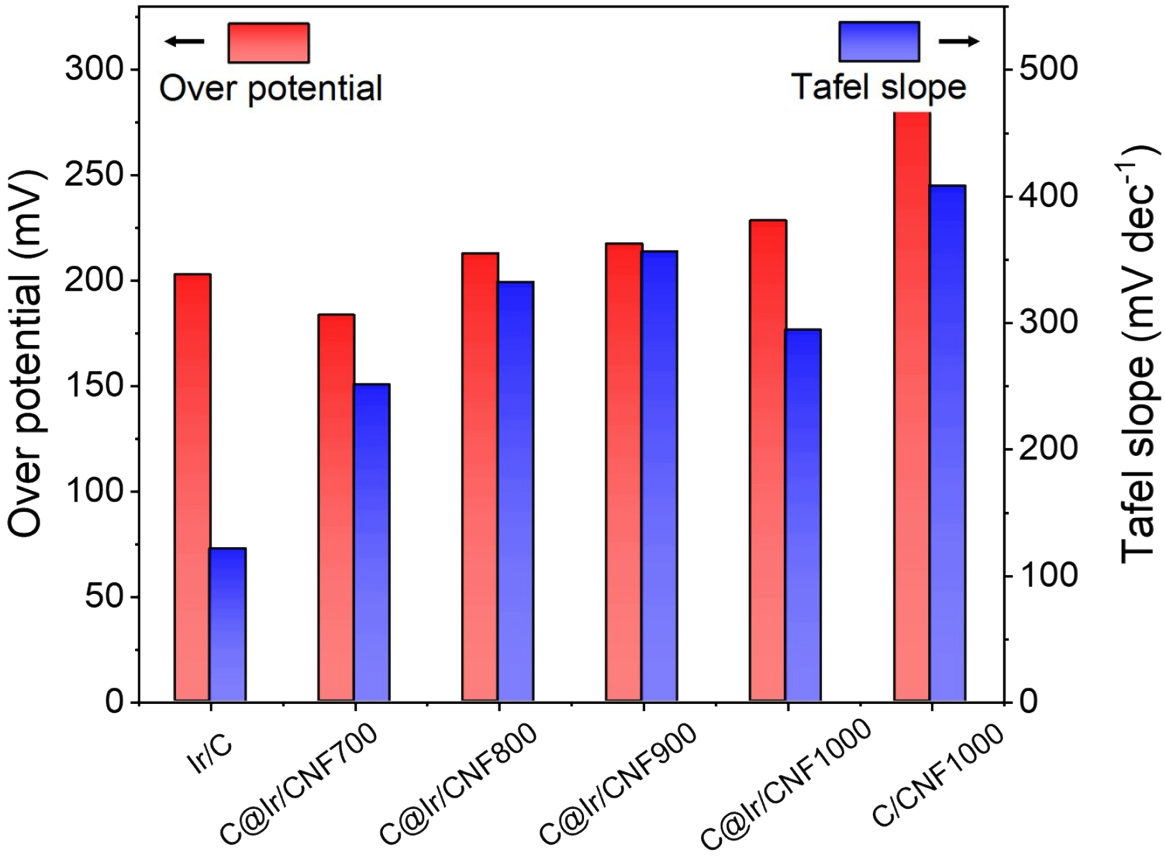

Fig. S8. Overpotential and Tafel slope values of Ir/C, C@Ir/CNF700, C@Ir/CNF800, C@Ir/CNF900, C@Ir/CNF1000, and C/CNF1000 from OER-LSV curves in Figures 4b and S5.

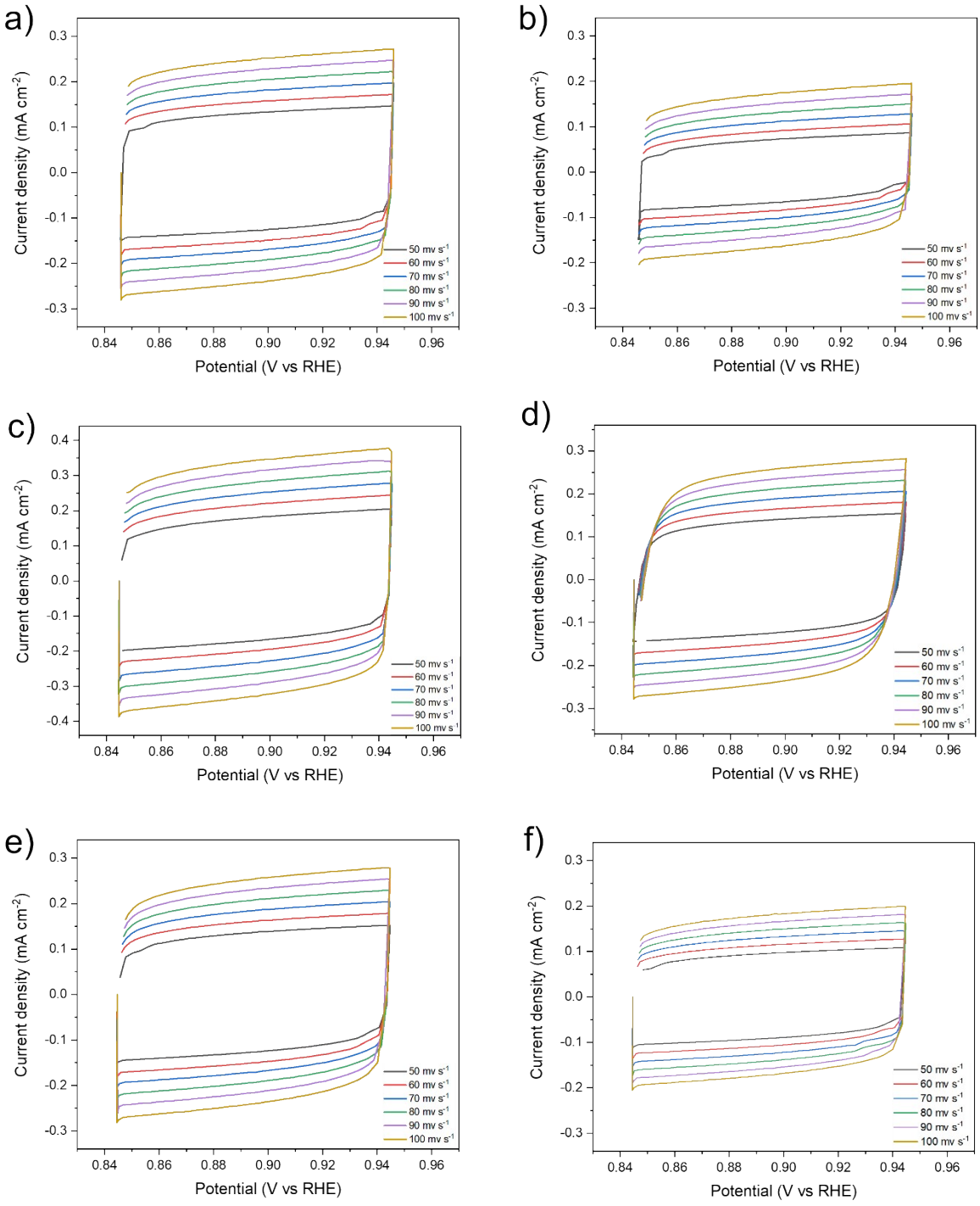

Fig. S9. EDLC at various scan rates for (a) Ir/C, (b) C/CNF1000, (c) C@Ir/CNF700, (d) C@Ir/CNF800, (e) C@Ir/CNF900, and (f) C@Ir/CNF1000.

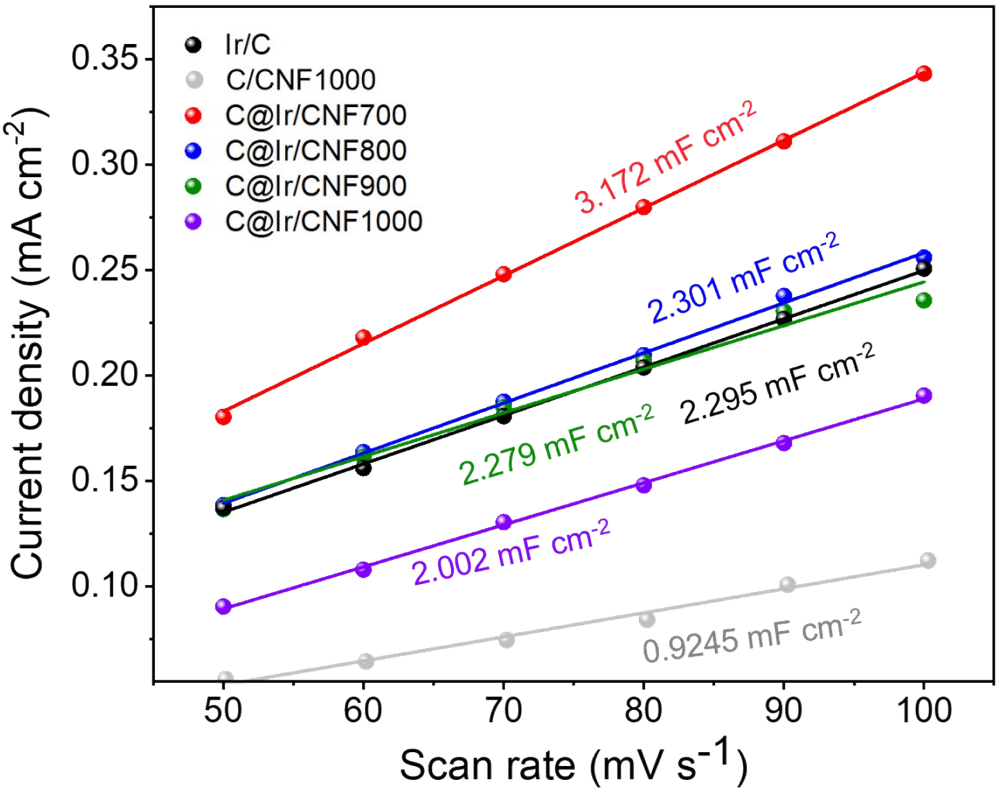

Fig. S10. Electrical double layer capacitance (EDLC) as a function of scan rate for C/CNF1000 compared to other C@Ir/CNF samples.

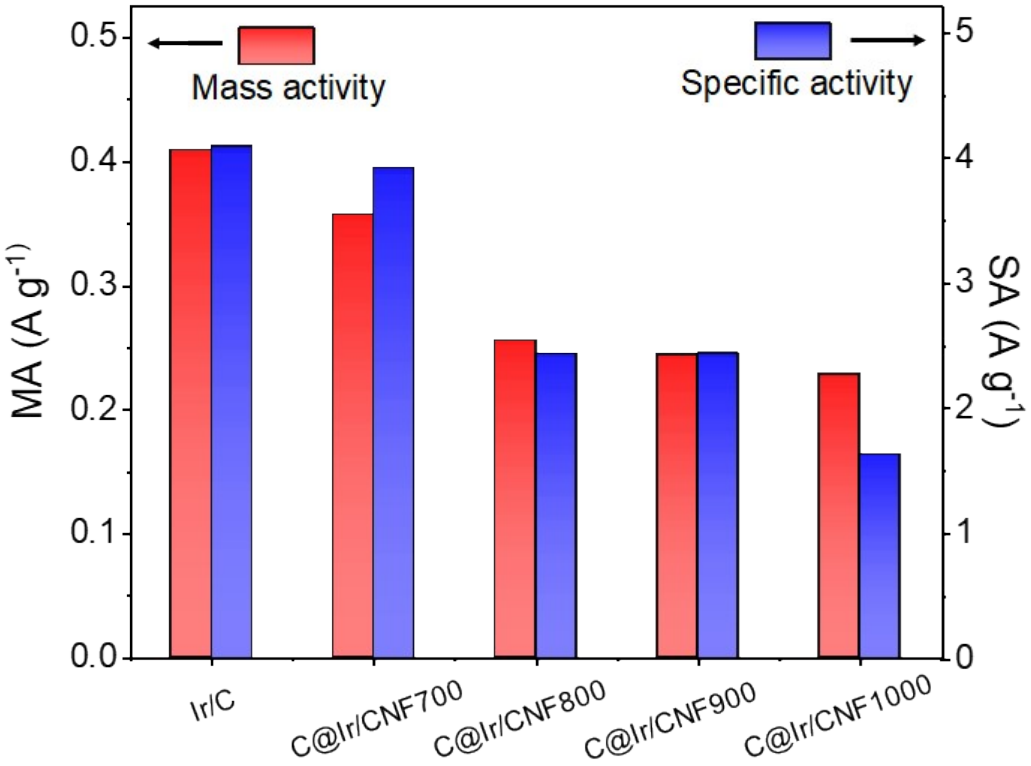

Fig. S11. Mass activity and specific activity from OER-LSV curves in Fig. 4b.

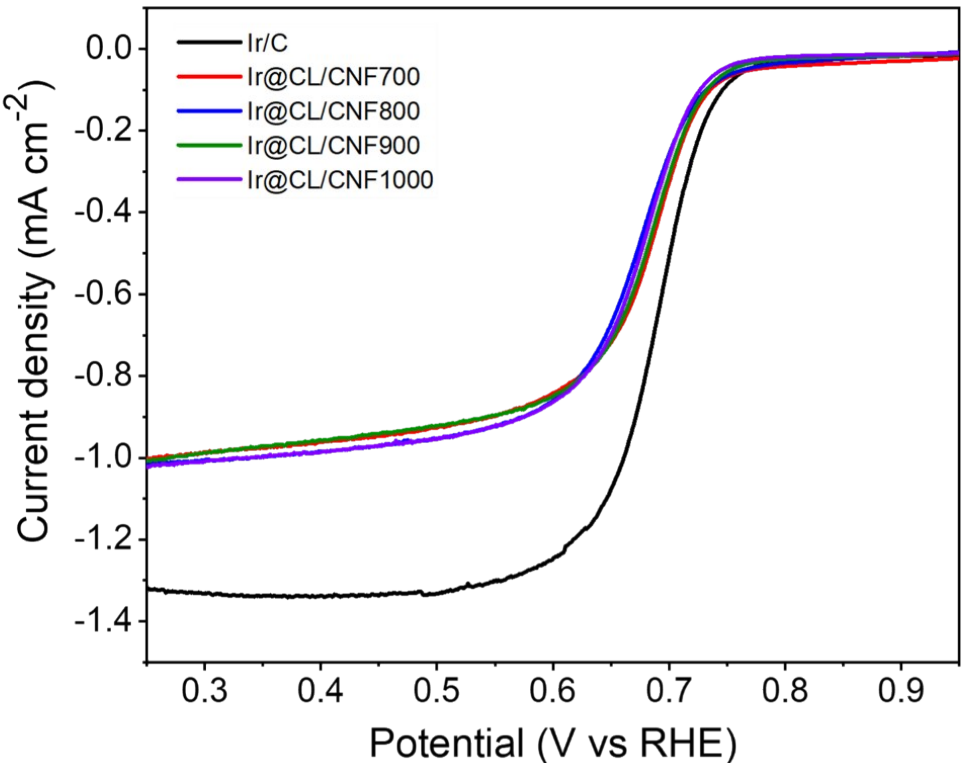

Fig. S12. ORR-LSV curves for Ir/C, C@Ir/CNF700, C@Ir/CNF800, C@Ir/CNF900, and C@Ir/CNF1000.

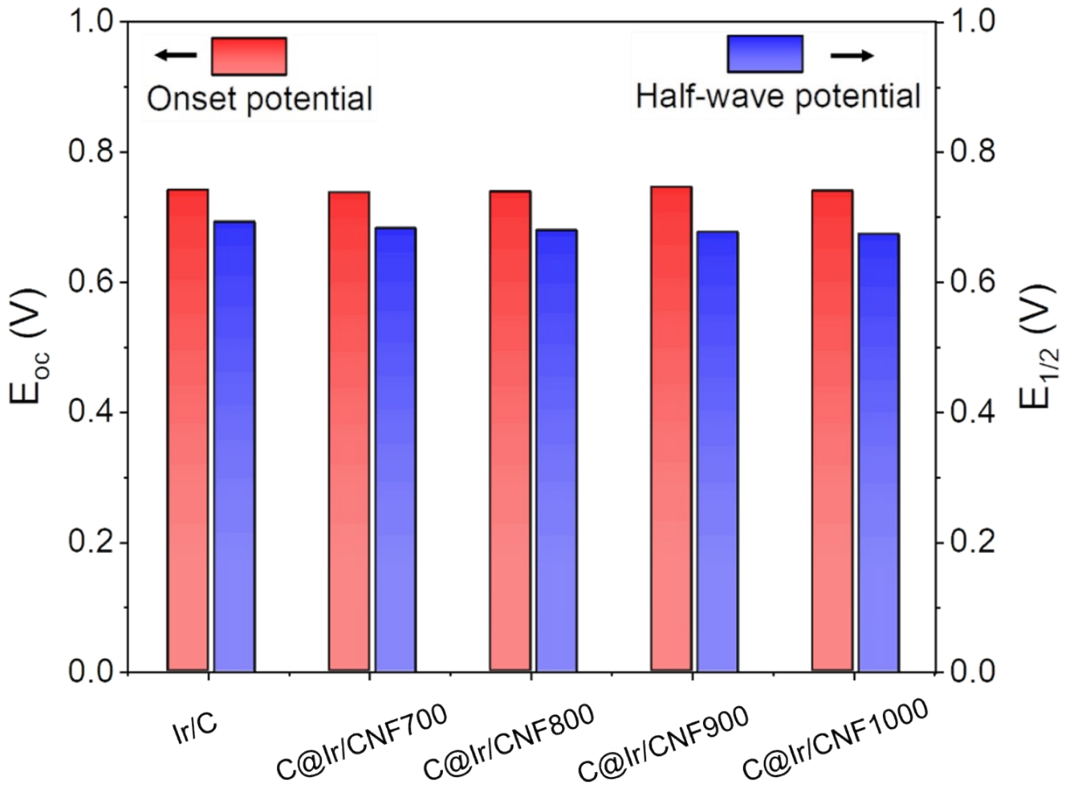

Fig. S13. Onset potential and half-wave potential values for Ir/C, C@Ir/CNF700, C@Ir/CNF800, C@Ir/CNF900, and C@Ir/CNF1000.

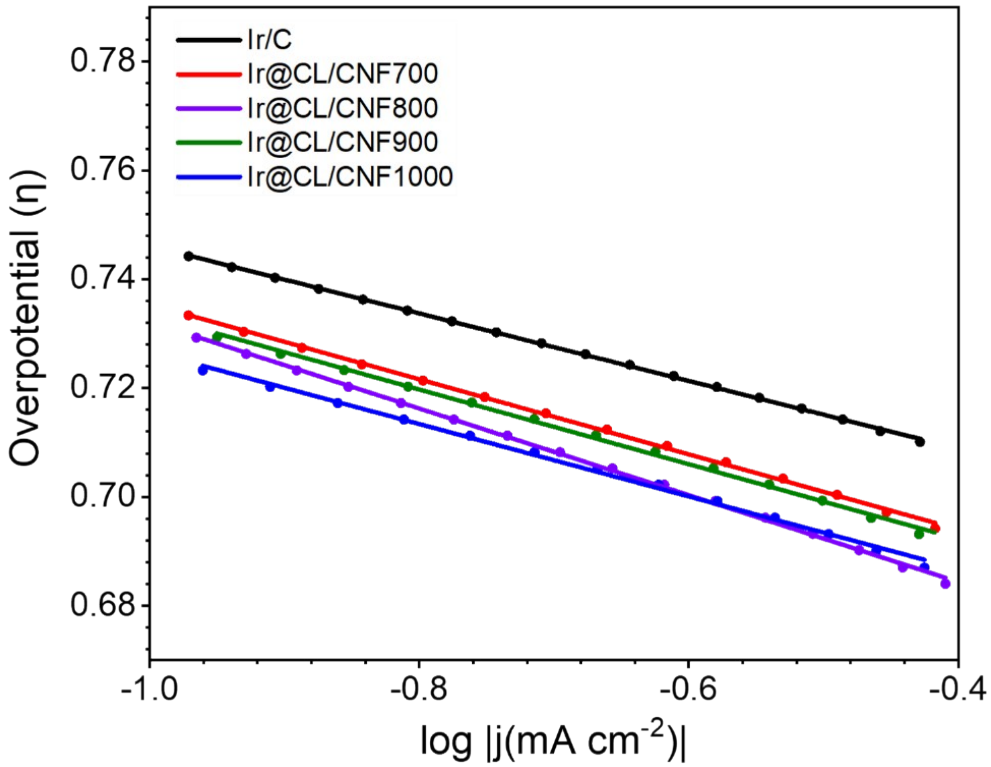

Fig. S14. Tafel plots for Ir/C, C@Ir/CNF700, C@Ir/CNF800, C@Ir/CNF900, and C@Ir/CNF1000 from ORR-LSV curves in Fig. S12.

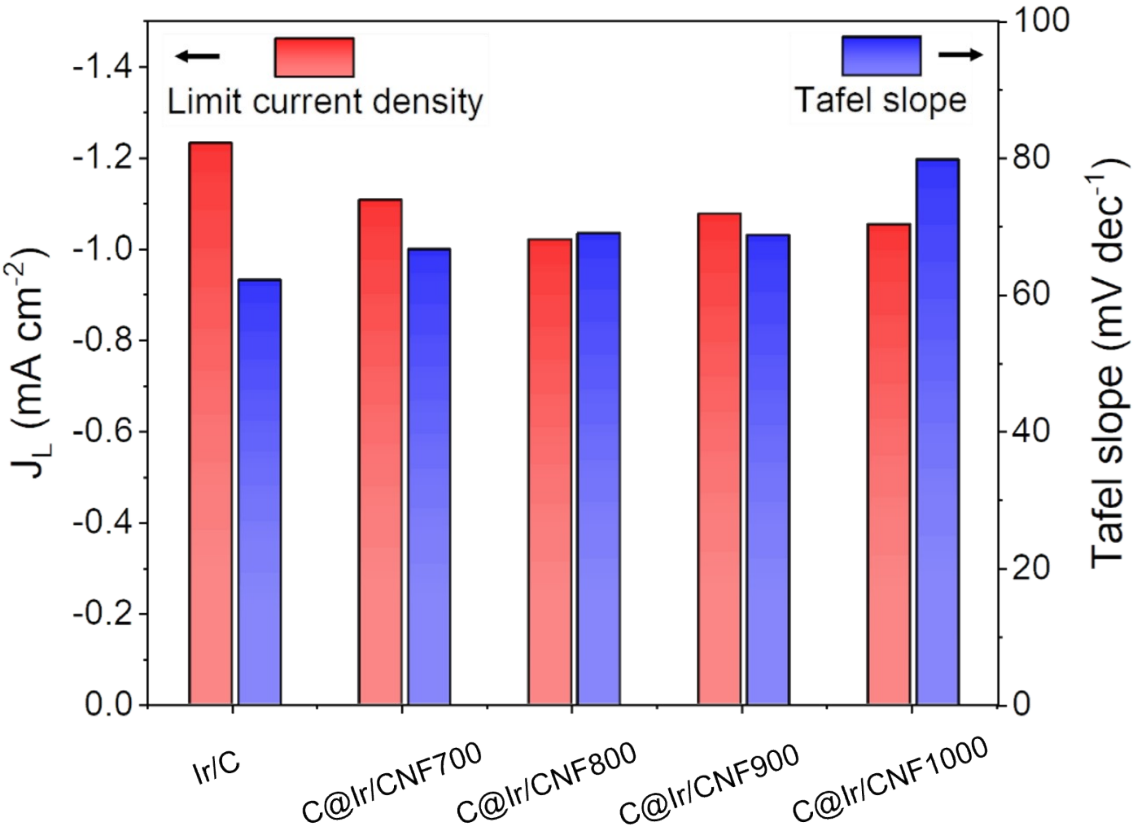

Fig. S15. Limit current density and Tafel slope values for Ir/C, C@Ir/CNF700, C@Ir/CNF800, C@Ir/CNF900, and C@Ir/CNF1000 from Figs. S12 and S14.

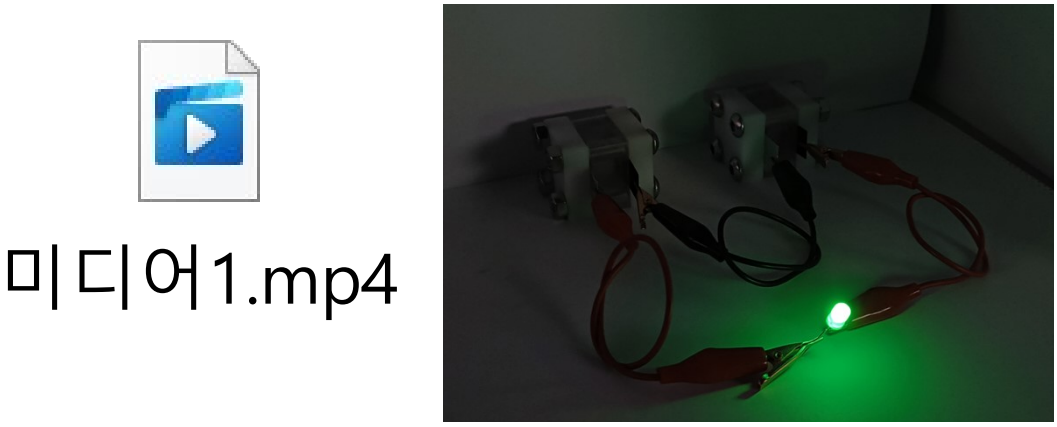

Fig. S16. A lighted green light-emitting diode (LED) powered by two series of homemade ZAB with C@Ir/CNF1000: (a) operation video, (b) digital image.

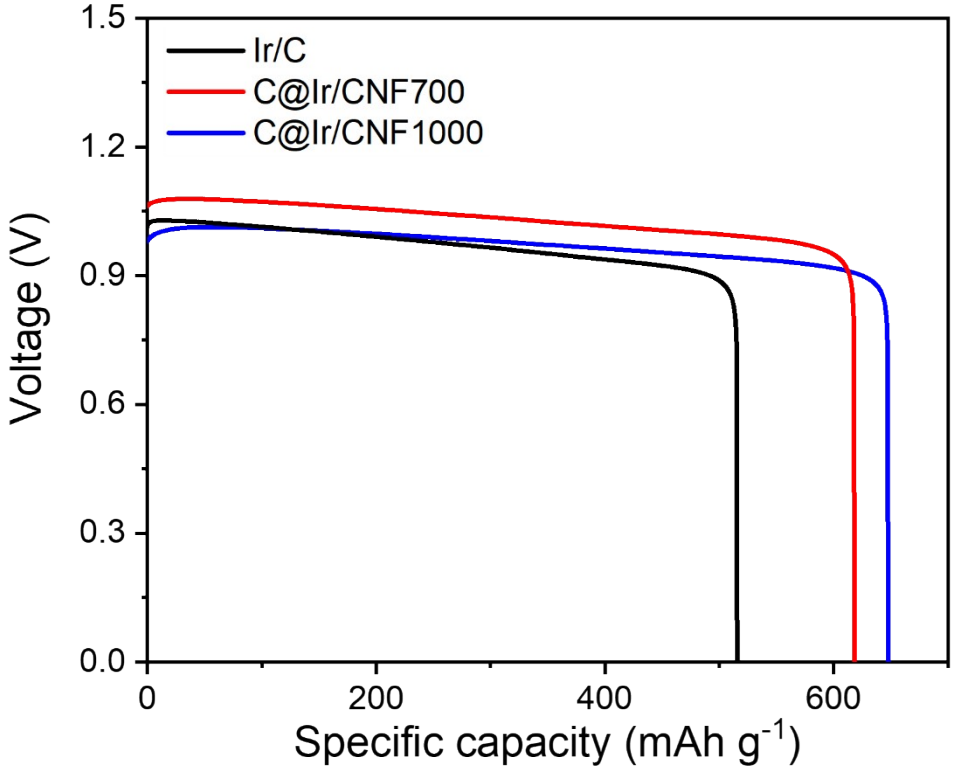

Fig. S17. Zn mass-normalized specific capacities at a current density of 25 mA cm^{-2}.

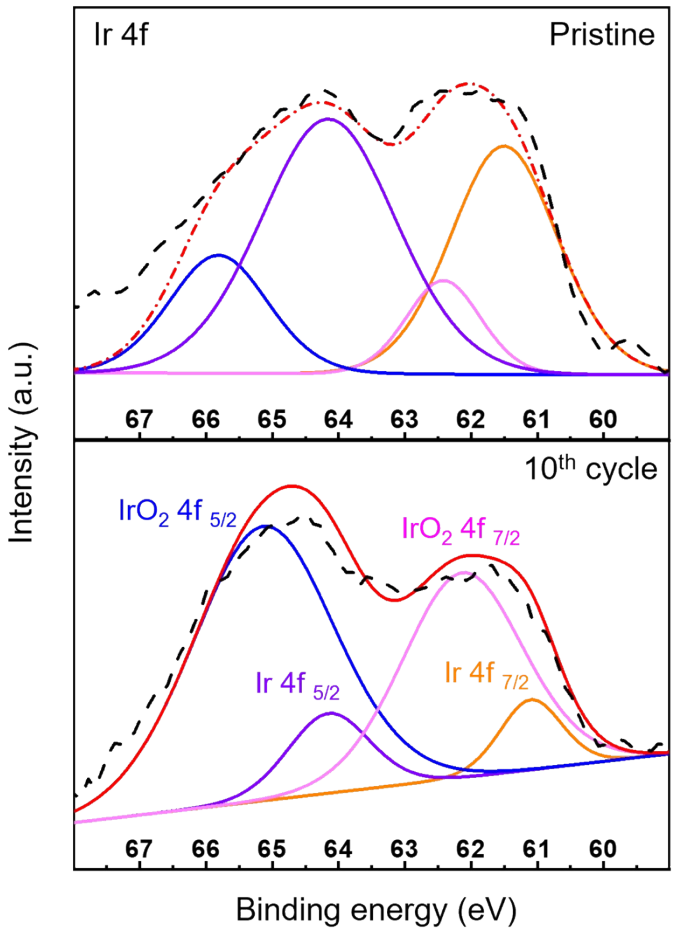

Fig. S18. Ir 4f XPS spectrum of the pristine state and after 10th cycle air cathode with C@Ir/CNF1000.

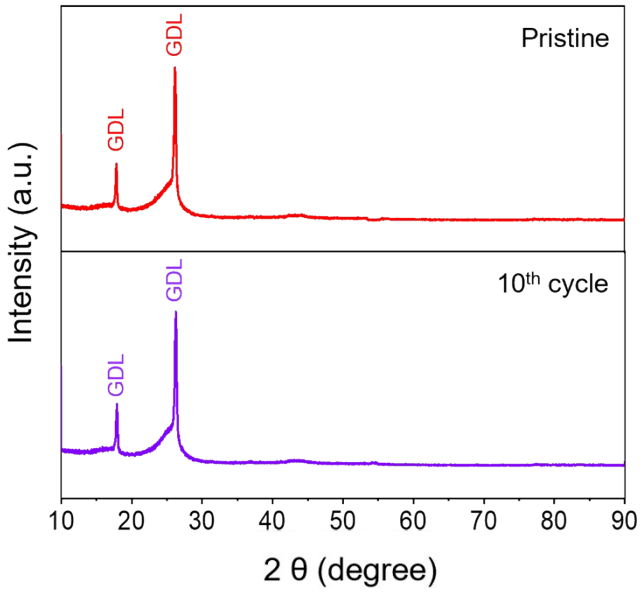

Fig. S19. XRD data of the pristine state and after 10th cycle air cathode with C@Ir/CNF1000.

Table S1. Calculated crystallite sizes using the Scherrer equation

$D_{hkl} = \frac{K\lambda}{\beta_{hkl}cos(\theta_{hkl})}$	**2θ (°)**	**Reflection Planes**	**FWHM (radian)**	**Crystallite size-*D* (nm)**
C@Ir/CNF800	40.9	(111)	4.98	1.78
C@Ir/CNF900			4.18	2.11
C@Ir/CNF1000			3.6	2.46

Table S2. Atomic and weight fractions of elements in C@Ir/CNF700 and C@Ir/CNF1000 from XPS analysis

		C	**Ir**	**N**	**O**
C@Ir/CNF700	At. %	72.47	3.69	12.76	11.08
	Wt. %	44.97	36.64	9.23	9.16
C@Ir/CNF1000	At. %	88.93	4.27	2.95	3.86
	Wt. %	53.62	41.20	2.07	3.10

Table S3. Comparison of ZAB performance with catalysts from other literature

Cathode catalyst	Cycling stability (hour (cycle))	Voltage gap (V)	Current density (mA cm^{-2})	Electrolyte	Ref
C@Ir/CNF	30 h (75 cycles)	0.936 V (0.973 V at the end)	5 mA cm^{-2}	6M KOH + 0.2M ZnAC	This work
FSZAB@Co-SAs/N–C/rGO	26.31 h (78 cycles)	≈0.8 V	1 mA cm^{-2}	6M KOH + 0.2M ZnAC	1
Single atom Ir embedded nitrogen -doped carbon	100 h (150 cycles)	~1.0 V	5 mA cm^{-2}	6M KOH + 0.2M ZnAC	2
MnO_2-NCNT	4 h (50 cycles)	increased ≈0.4 V at the end	8 mA cm^{-2}	6M KOH	3
$CoMn_2O_4$/N-rGO	80 h (1200 cycles)	Increased ≈0.2 V at the end	5 mA cm^{-2}	6M KOH	4
Co_3O_4/carbon nanofibers	135 h (135 cycles)	Increased ≈0.08 V at the end	1 mA cm^{-2}	6M KOH + 0.2M $ZnCl_2$	5
Co/NC	12 h	0.88 V	5 $mAcm^{-2}$	6M KOH	6
3d-GMC	200 h (120 cycles)	≈0.8 V (≈1.0 V at the end)	5 mA cm^{-2}	6M KOH + 0.2M ZnAC	7
SA-Fe-SNC@900	160 h (960 cycles)	0.75 V (0.84 V at the end)	5 mA cm^{-2}	6M KOH + 0.2M ZnAC	8
CuNCs–CoNCs/NPCF	20 h (5000 cycles)	0.8 V (0.82 V at the end)	10 mA cm^{-2}	6M KOH + 0.2M ZnAC	9
POP-Fe/Ni-900	120 h (450 cycles)	≈0.65 V (≈0.75 V at the end)	5 mA cm^{-2}	6M KOH + 0.2M ZnAC	10
NiCu–MoS_2	133 h (400 cycles)	0.71 V (0.74 V at the end)	5 $mAcm^{-2}$	6M KOH + 0.2M ZnAC	11
Fe_3Co-NC@900	675 cycles	0.898 V (1.045 V at the end)	10 mA cm^{-2}	6M KOH + 0.02 M ZnAC	12
Fe-SA@NC-2	60 h	0.8 V at the end	1 mA cm^{-2}	6M KOH + 0.2M ZnAC	13

Supporting information references

1. L. Li, N. Li, J. Xia, S. Zhou, X. Qian, F. Yin, G. He and H. Chen, *J. Mater. Chem. A*, 2023, **11**, 2291-2301.
2. X. Luo, M. Yang, W. Song, Q. Fang, X. Wei, L. Jiao, W. Xu, Y. Kang, H. Wang, N. Wu, W. Gu, L. Zheng, L. Hu and C. Zhu, *Adv. Funct. Mater.*, 2021, **31**, 2101193.
3. Z. Chen, A. Yu, R. Ahmed, H. Wang, H. Li and Z. Chen, *Electrochim. Acta*, 2012, **69**, 295-300.
4. Y. Liang, Q. Gong, X. Sun, N. Xu, P. Gong and J. Qiao, *Funct. Mater. Lett.*, 2020, **13**, 8.
5. X. Sun, T. Xu, W. Sun, J. Bai and C. Li, *J. Alloys Compd.*, 2022, **898**, 162778.
6. R. Wang, H. Yang, N. Lu, S. Lei, D. Jia, Z. Wang, Z. Liu, X. Wu, H. Zheng, S. Ali, F. Ma and S. Peng, *Chem. Eng. J.*, 2022, **433**, 134500.
7. S. J. Ha, J. Hwang, M. J. Kwak, J. C. Yoon and J. H. Jang, *Small*, 2023, **19**, 2300551.
8. Z. Chen, X. Peng, Z. Chen, T. Li, R. Zou, G. Shi, Y. Huang, P. Cui, J. Yu, Y. Chen, X. Chi, K. P. Loh, Z. Liu, X. Li, L. Zhong and J. Lu, *Adv. Mater*, 2023, **35**, 2209948.
9. Q. Dong, H. Wang, F. Liu, J. Ren, H. Wang, X. Wang and R. Wang, *J. Mater. Chem. A*, 2023, **11**, 4717-4728.
10. P. Weng, Y. Guo, K. Wu, X. Wang, G.-Q. Huang, H. Lei, Y. Yuan, W. Lu and D. Li, *J. Mater. Chem. A*, 2023, **11**, 12194-12201.
11. M. Kumar and T. C. Nagaiah, *J. Mater. Chem. A*, 2023, **11**, 18336-18348.
12. K. Srinivas, H. Yu, Z. Chen, A. Chen, M.-q. Zhu, Y. Chen and C. Yang, *J. Mater. Chem. A*, 2024, **12**, 16863-16876.
13. J.-F. Gu, J. Wang, Q. Wu, C. Wang, F. Verpoort and S. Chaemchuen, *J. Mater. Chem. A*, 2024, **12**, 16528-16536.